Published in final edited form as:

Nature. 2011 January 20; 469(7330): 424–427. doi:10.1038/nature09640.

Atomic level modeling of the HIV capsid

Owen Pornillos[1,2], **Barbie K. Ganser-Pornillos**[1,2], and **Mark Yeager**[1,2,3]

[1] Department of Molecular Physiology and Biological Physics, University of VirginiaSchool of Medicine, Charlottesville, Virginia 22908, USA

[2] Department of Cell Biology, The Scripps Research Institute, La Jolla, California 92037, USA

[3] Division of Cardiovascular Medicine, Department of Medicine, University of VirginiaHealth System, Charlottesville, Virginia 22908, USA

Abstract

The mature capsids of human immunodeficiency virus type 1 (HIV-1) and other retroviruses are fullerene shells, composed of the viral CA protein, that enclose the viral genome and facilitate its delivery into new host cells1. Retroviral CA proteins contain independently-folded N-terminal and C-terminal domains (NTD and CTD) that are connected by a flexible linker2–4. The NTD forms either hexameric or pentameric rings, whereas the CTD forms symmetric homodimers that connect the rings into a hexagonal lattice3,5–13. We previously used a disulfide crosslinking strategy to enable isolation and crystallization of soluble HIV-1 CA hexamers11,14. By the same approach, we have now determined the X-ray structure of the HIV-1 CA pentamer at 2.5 Å resolution. Two mutant CA proteins with engineered disulfides at different positions (P17C/T19C and N21C/A22C) converged onto the same quaternary structure, indicating that the disulfide-crosslinked proteins recapitulate the structure of the native pentamer. Assembly of the quasi-equivalent hexamers and pentamers requires remarkably subtle rearrangements in subunit interactions, and appears to be controlled by an electrostatic switch that favors hexamers over pentamers. This study completes the gallery of sub-structures describing the components of the HIV-1 capsid and enables atomic level modeling of the complete capsid. Rigid-body rotations around two assembly interfaces appear sufficient to generate the full range of continuously varying lattice curvature in the fullerene cone.

By analogy to quasi-equivalent icosahedral virus capsids, the subunits of the conical fullerene capsid of HIV-1 are organized on a hexagonal lattice that requires insertion of

Correspondence should be addressed to M.Y. (yeager@virginia.edu).

Full Methods and any associated references are available in the online version of the paper at www.nature.com/nature.

Supplementary Information is linked to the online version of the paper at www.nature.com/nature.

Author Contributions. All authors designed/performed the experiments, analyzed the data, and wrote the manuscript. O.P. performed the computational aspects of crystallographic structure determination.

Author Information. Coordinates and structure factors are available from the PDB database (www.rcsb.org): 3P05, N21C/A22C-stabilized pentamer; 3P0A, P17C/T19C-stabilized pentamer. To properly reflect the limited resolution of the second structure, only Cα coordinates were deposited. The authors declare no competing financial interests. Reprints and permissions information is available at www.nature.com/reprints. Readers are welcome to comment on the online version of this paper at www.nature.com/nature.

exactly 12 pentamers to close the shell6,15–17. However, the pentamers in an icosahedral capsid are in a symmetric configuration at the vertices, whereas pentamers in the fullerene cone are distributed asymmetrically, with 5 at the narrow end and 7 at the wide end15. The Rous sarcoma retrovirus (RSV) CA protein can form icosahedrally symmetric particles *in vitro*, and electron cryomicroscopy maps at 10 Å resolution indicate that the hexamer and pentamer are indeed quasi-equivalent; that is, RSV CA forms both oligomers using the same interacting surfaces9,13.

We previously used a disulfide crosslinking strategy to facilitate purification and structure determination of HIV-1 CA hexamers11,14. To explore the molecular basis of retroviral CA quasi-equivalence, we have now determined X-ray structures of two disulfide-crosslinked HIV-1 CA pentamers at 2.5 and 6 Å resolution (Supplementary Figs. 1 and 2, Supplementary Table 1). The independent pentamer structures were closely superimposable (Supplementary Fig. 3). Therefore, the crosslinked proteins likely recapitulate the native pentameric architecture of HIV-1 CA. The structures were also similar to the lower resolution structures of the RSV CA pentamer9,13.

Comparison of the new pentamer structures with the HIV-1 CA hexamer structures8,11,14 confirms that the two oligomers are highly related (Fig. 1). In both cases, the CTDs form a “belt” (blue in Fig. 1a, d) surrounding the inner ring of NTDs (orange). The NTD and CTD of each CA molecule cradle the NTD from the neighboring subunit (illustrated for the pentamer in Fig. 1b, c; for the hexamer in Fig. 1e, f; and for both oligomers in superposition in Fig. 2a). Intermolecular NTD-NTD interactions facilitate formation of the NTD rings, whereas NTD-CTD interactions hold the CTD subunits in the “belts” against the inner NTD rings. There are no intramolecular interactions between the NTD and CTD of each subunit, apart from the covalent peptide linkage between these domains (red arrowhead in Fig. 2a). The ability of the inherently flexible linker to adopt different conformations facilitates appropriate juxtaposition of the same interaction surfaces in both the pentamer and hexamer.

Previous analysis indicated that the hexameric NTD ring closely obeys 6-fold rotational symmetry and is relatively rigid, whereas the CTD subunits in the “belts” are mobile and can rotate relative to the NTD ring11. Each CTD pivots as a rigid body about four intermolecular helix-capping hydrogen bonds at the NTD-CTD interface. With these motions, each hexameric ring can adopt slightly different dihedral angles relative to its adjacent rings in the capsid lattice9,11,12. The NTD-CTD interfaces within the pentamer and hexamer are remarkably similar (Fig. 2b). Indeed, comparison of the crystallographically distinct pentamers reveals the same type and degree of flexibility as the hexamer (i.e., the 5-fold symmetric NTD ring is apparently rigid, and the CTDs are more mobile) (Fig. 2c and Supplementary Fig. 3). These results indicate that the pentamer and hexamer use the same mechanism to accommodate local variations in capsid lattice curvature.

NTD ring interactions are mediated by the first three α-helices of each subunit, which form a 15-helix barrel in the pentamer (Fig. 3a) and an 18-helix barrel in the hexamer (Fig. 3b). There are subtle differences in the repeating set of NTD-NTD contacts, which comprise a 3-helix bundle, with helix 2 of one subunit (orange in Fig. 3c) packed length-wise against

helices 1 and 3 of the adjacent subunit (blue). Aliphatic sidechains at the center of the bundle form a small hydrophobic core, whereas polar residues at the periphery participate in hydrophilic interactions. As noted previously, direct hydrophilic protein-protein contacts are conspicuously absent in the hexameric NTD ring, and essentially all the intersubunit hydrogen bonds are bridged by ordered water molecules11. In the pentamer structure, ordered waters were not modeled (see Methods), but examination of residual difference density indicates that the assembly interfaces are likewise solvated (not shown).

The 5-fold and 6-fold symmetric NTD rings are distinguished through the angle subtended by adjacent subunits (72° in the pentamer and 60° in the hexamer, with the angle vertex at the center of each ring) (Fig. 3a, b). To a first approximation, this difference is accommodated by a simple rotation of the subunits relative to each other (Fig. 3d). Remarkably, the rotation axis appears to coincide with the center of the 3-helix bundle (red dot in Fig. 3d), which allows essentially equivalent packing of the aliphatic residues. Thus, the hydrophobic NTD-NTD interactions are conserved in the two rings. In contrast, the polar atoms at the outer edges of the 3-helix bundle display substantially different interatomic distances, but compensatory movements of water molecules appear to maintain ring-stabilizing hydrogen bonds (not shown). Our structures therefore indicate that switching between the CA hexamer and pentamer occurs via subtle changes in intersubunit bonding interactions, and follow the principles of quasi-equivalence as originally envisioned by Caspar and Klug18.

Pentamer formation brings charged residues at the center of the ring in close proximity, inducing both attractive and repulsive ionic interactions. This implies that electrostatic forces control switching between the pentamer and hexamer, as was suggested for RSV CA9. For the HIV-1 CA oligomers, the points of closest approach occur at an annulus at the top of helix 1, which is occupied by an arginine residue (Arg18) (Supplementary Fig. 4). The arginines appear well accommodated within the annulus of the hexamer, but in contrast, are more closely apposed in the pentamer. Closer juxtaposition of like charges is expected to create stronger electrostatic repulsion, which is consistent with the biochemical observation that assembly of HIV-1 CA pentamers is disfavored relative to hexamers. Elimination of the charge is expected to favor pentamer formation, and indeed, mutation of Arg18 into alanine promotes assembly of highly curved particles (cones, spheres, spirals, short capped cylinders)19. In contrast, wild-type CA typically assembles into long tubes composed of hexamers20–22. Mutation of Arg18 to valine, isoleucine, or leucine induces assembly of spheres (i.e., more efficient pentamer formation)8, and we presume that this is because the larger aliphatic sidechains contribute stabilizing hydrophobic contacts.

The importance of Arg18 for the energetic landscape of HIV-1 CA assembly is consistent with its very high degree of conservation (99.8% of 2,460 sequences in the Los Alamos database)23. We propose that electrostatic destabilization of the pentamer is precisely counterbalanced by cooperative lattice stabilization, such that pentamers form and integrate into the assembling capsid only when required to relieve strain induced by local lattice curvature. We further speculate that the narrow end of the cone may be particularly susceptible to destabilization because this region has a high concentration of pentamers, and this may be relevant to capsid disassembly or uncoating.

At this time, it is not possible to experimentally determine the atomic structure of the native HIV-1 capsid. Nevertheless, having on hand a complete gallery of high-resolution structures of the building blocks allowed us to model a fullerene cone capsid (Fig. 4a). In our modeling, the NTD hexamers, NTD pentamers, and CTD dimers were treated as rigid bodies, and intersubunit distances across the NTD-CTD interfaces were used as indicators of model quality (see Methods) (Fig. 4b).

Within the body of the cone, the CA subunits were arranged on a hexagonal lattice with a unit cell spacing of ~93 Å. Consistent with a previous proposal11, we found that the full range of variable lattice curvature in this region could be modeled by introducing small rigid-body rotations across the NTD-CTD interfaces, while keeping the NTD-NTD hexamerization and CTD-CTD dimerization interfaces constant. In modeling the pentameric declinations, wherein the lattice curvature is most pronounced, we found that the CTD dimers must span different distances when connecting hexamers to hexamers (~33 Å) and hexamers to pentamers (~26 Å) (Supplementary Fig. 5a). These distances are in close correspondence to the dimensions of two independently-determined CTD dimer structures, 2KOD12 and 1A435, and suggests a rationale for the seemingly disparate structures of the dimers. Although the structures were solved from slightly different protein constructs, both retained the dimerization affinity of full-length CA3,12. However, each exhibited a distinct subunit packing geometry across the dimer dyad (Supplementary Fig. 5b). Therefore, the 2KOD dimer was used to connect hexamers to hexamers, and the 1A43 dimer was used to connect hexamers to pentamers. Models wherein the NTD rings were connected by either dimer alone displayed significant backbone clashes (2KOD) or relatively large separations (1A43) between subunits surrounding the declinations (not shown). This suggests that rotation or slippage at the CTD-CTD interface may be a mechanistic element of capsid assembly, which is consistent with studies showing that the CTD has a flexible architecture4,24–28.

It is remarkable that our simple modeling approach, which allowed just two types of rigid-body rotations between the building blocks, produced a fullerene model wherein essentially all the subunits displayed reasonable packing geometries. On the basis of this analysis, we conclude that CA assembly entails flexibility at both the NTD-CTD interface and the dimer interface to generate the constantly varying lattice curvature in the HIV-1 capsid.

METHODS SUMMARY

Soluble, disulfide-crosslinked pentamers of HIV-$1_{NL4–3}$ CA (containing either N21C/A22C/W184A/M185A or P17C/R18L/T19C/W184A/M185A mutations) were prepared by sequential dialysis of purified protein. Crystals were obtained by the sitting-drop vapor diffusion method in Tris-buffered precipitant solutions containing polyethylene glycol and sodium iodide. Synchrotron diffraction data were processed with the program HKL2000. Molecular replacement phasing, model building, and crystallographic refinement were performed with the programs MOLREP, Coot, and PHENIX. The capsid model was built by manual rigid-body docking of the high-resolution structures of the 5-fold symmetric NTD ring (PDB code 3P05), the 6-fold symmetric NTD ring (3H47), and 2-fold symmetric CTD dimers (2KOD and 1A43) into a geometric fullerene cone model.

Supplementary Material

Refer to Web version on PubMed Central for supplementary material.

Acknowledgments

This study was funded by U.S. National Institutes of Health grants to M.Y. (R01-GM066087 and P50-GM082545). X-ray diffraction data were collected at beamlines 22-BM and 22-ID at Advanced Photon Source, Argonne National Laboratory. Initial crystal screening was performed with the expert assistance of Sankaran Banumathi through the Collaborative Crystallography Program, Lawrence Berkeley National Laboratory at the Advanced Light Source. We thank John E. Johnson and Dominica Borek for crystallographic advice; Yuanzi Hua for assistance with molecular biology experiments; and Ian Wilson, Chris Hill, and Wes Sundquist for critical reading of the manuscript.

References

1. Ganser-Pornillos BK, Yeager M, Sundquist WI. The structural biology of HIV assembly. Curr Opin Struct Biol. 2008; 18:203–217. [PubMed: 18406133]
2. Gitti RK, et al. Structure of the amino-terminal core domain of the HIV-1 capsid protein. Science. 1996; 273:231–235. [PubMed: 8662505]
3. Gamble TR, et al. Structure of the carboxyl-terminal dimerization domain of the HIV-1 capsid protein. Science. 1997; 278:849–853. [PubMed: 9346481]
4. Berthet-Colominas C, et al. Head-to-tail dimers and interdomain flexibility revealed by the crystal structure of HIV-1 capsid protein (p24) complexed with a monoclonal antibody Fab. EMBO J. 1999; 18:1124–1136. [PubMed: 10064580]
5. Worthylake DK, Wang H, Yoo S, Sundquist WI, Hill CP. Structures of the HIV-1 capsid protein dimerization domain at 2.6 A resolution. Acta Crystallogr D Biol Crystallogr. 1999; 55:85–92. [PubMed: 10089398]
6. Li S, Hill CP, Sundquist WI, Finch JT. Image reconstructions of helical assemblies of the HIV-1 CA protein. Nature. 2000; 407:409–413. [PubMed: 11014200]
7. Mortuza GB, et al. High-resolution structure of a retroviral capsid hexameric amino-terminal domain. Nature. 2004; 431:481–485. [PubMed: 15386017]
8. Ganser-Pornillos BK, Cheng A, Yeager M. Structure of full-length HIV-1 CA: a model for the mature capsid lattice. Cell. 2007; 131:70–79. [PubMed: 17923088]
9. Cardone G, Purdy JG, Cheng N, Craven RC, Steven AC. Visualization of a missing link in retrovirus capsid assembly. Nature. 2009; 457:694–698. [PubMed: 19194444]
10. Bailey GD, Hyun JK, Mitra AK, Kingston RL. Proton-linked dimerization of a retroviral capsid protein initiates capsid assembly. Structure. 2009; 17:737–748. [PubMed: 19446529]
11. Pornillos O, et al. X-ray structures of the hexameric building block of the HIV capsid. Cell. 2009; 137:1282–1292. [PubMed: 19523676]
12. Byeon IJ, et al. Structural convergence between cryoEM and NMR reveals intersubunit interactions critical for HIV-1 capsid function. Cell. 2009; 139:780–790. [PubMed: 19914170]
13. Hyun JK, Radjainia M, Kingston RL, Mitra AK. Proton-driven assembly of the Rous sarcoma virus capsid protein results in the formation of icosahedral particles. J Biol Chem. 2010; 285:15056–15064. [PubMed: 20228062]
14. Pornillos O, Ganser-Pornillos BK, Banumathi S, Hua Y, Yeager M. Disulfide bond stabilization of the hexameric capsomer of human immunodeficiency virus. J Mol Biol. 2010; 401:985–995. [PubMed: 20600115]
15. Ganser BK, Li S, Klishko VY, Finch JT, Sundquist WI. Assembly and analysis of conical models for the HIV-1 core. Science. 1999; 283:80–83. [PubMed: 9872746]
16. Jin Z, Jin L, Peterson DL, Lawson CL. Model for lentivirus capsid core assembly based on crystal dimers of EIAV p26. J Mol Biol. 1999; 286:83–93. [PubMed: 9931251]

17. Heymann JB, Butan C, Winkler DC, Craven RC, Steven AC. Irregular and semi-regular polyhedral models for Rous sarcoma virus cores. Comput Math Methods Med. 2008; 9:197–210. [PubMed: 19122884]
18. Caspar DL, Klug A. Physical principles in the construction of regular viruses. Cold Spring Harb Symp Quant Biol. 1962; 27:1–24. [PubMed: 14019094]
19. Ganser-Pornillos BK, von Schwedler UK, Stray KM, Aiken C, Sundquist WI. Assembly properties of the human immunodeficiency virus type 1 CA protein. J Virol. 2004; 78:2545–2552. [PubMed: 14963157]
20. Ehrlich LS, Agresta BE, Carter CA. Assembly of recombinant human immunodeficiency virus type 1 capsid protein *in vitro*. J Virol. 1992; 66:4874–4883. [PubMed: 1629958]
21. Campbell S, Vogt VM. Self-assembly *in vitro* of purified CA-NC proteins from Rous sarcoma virus and human immunodeficiency virus type 1. J Virol. 1995; 69:6487–6497. [PubMed: 7666550]
22. Gross I, Hohenberg H, Krausslich HG. In vitro assembly properties of purified bacterially expressed capsid proteins of human immunodeficiency virus. Eur J Biochem. 1997; 249:592–600. [PubMed: 9370371]
23. http://www.hiv.lanl.gov/content/index.
24. Ternois F, Sticht J, Duquerroy S, Krausslich HG, Rey FA. The HIV-1 capsid protein C-terminal domain in complex with a virus assembly inhibitor. Nat Struct Mol Biol. 2005; 12:678–682. [PubMed: 16041386]
25. Ivanov D, et al. Domain-swapped dimerization of the HIV-1 capsid C-terminal domain. Proc Natl Acad Sci USA. 2007; 104:4353–4358. [PubMed: 17360528]
26. Alcaraz LA, del Alamo M, Barrera FN, Mateu MG, Neira JL. Flexibility in HIV-1 assembly subunits: solution structure of the monomeric C-terminal domain of the capsid protein. Biophys J. 2007; 93:1264–1276. [PubMed: 17526561]
27. Bartonova V, et al. Residues in the HIV-1 capsid assembly inhibitor binding site are essential for maintaining the assembly-competent quaternary structure of the capsid protein. J Biol Chem. 2008; 283:32024–32033. [PubMed: 18772135]
28. Wong HC, Shin R, Krishna NR. Solution structure of a double mutant of the carboxy-terminal dimerization domain of the HIV-1 capsid protein. Biochemistry. 2008; 47:2289–2297. [PubMed: 18220423]
29. von Schwedler UK, Stray KM, Garrus JE, Sundquist WI. Functional surfaces of the human immunodeficiency virus type 1 capsid protein. J Virol. 2003; 77:5439–5450. [PubMed: 12692245]
30. Otwinowski Z, Minor W. Processing of X-ray diffraction data collected in oscillation mode. Methods Enzymol. 1997; 276:307–326.
31. Vagin A, Teplyakov A. MOLREP: an automated program for molecular replacement. J Appl Cryst. 1997; 30:1022–1025.
32. Emsley P, Lohkamp B, Scott WG, Cowtan K. Features and development of Coot. Acta Crystallogr D Biol Crystallogr. 2010; 66:486–501. [PubMed: 20383002]
33. Reddy V, et al. Effective electron-density map improvement and structure validation on a Linux multi-CPU web cluster: The TB Structural Genomics Consortium Bias Removal Web Service. Acta Crystallogr D Biol Crystallogr. 2003; 59:2200–2210. [PubMed: 14646078]
34. Adams PD, et al. PHENIX: building new software for automated crystallographic structure determination. Acta Crystallogr D Biol Crystallogr. 2002; 58:1948–1954. [PubMed: 12393927]
35. Kleywegt GJ, Jones T. A xdlMAPMAN and xdlDATAMAN - programs for reformatting, analysis and manipulation of biomacromolecular electron-density maps and reflection data sets. Acta Crystallogr D Biol Crystallogr. 1996; 52:826–828. [PubMed: 15299647]
36. Vaguine AA, Richelle J, Wodak SJ. SFCHECK: a unified set of procedures for evaluating the quality of macromolecular structure-factor data and their agreement with the atomic model. Acta Crystallogr D Biol Crystallogr. 1999; 55:191–205. [PubMed: 10089410]
37. Chen VB, et al. MolProbity: all-atom structure validation for macromolecular crystallography. Acta Crystallogr D Biol Crystallogr. 2010; 66:12–21. [PubMed: 20057044]
38. Wriggers W, Schulten K. Protein domain movements: detection of rigid domains and visualization of hinges in comparisons of atomic coordinates. Proteins. 1997; 29:1–14. [PubMed: 9294863]

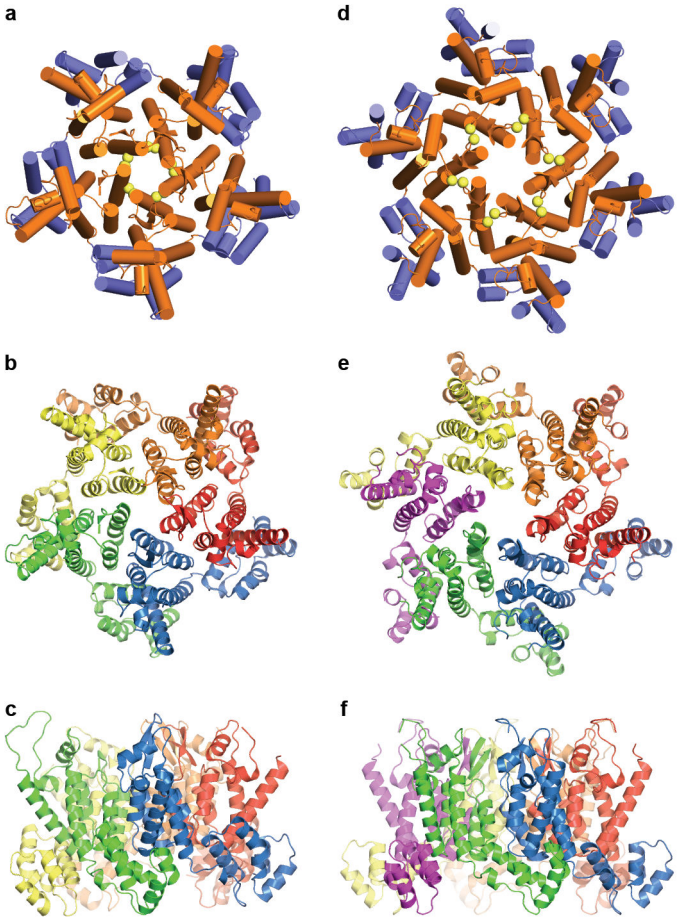

Figure 1. Structure of the disulfide-stabilized HIV-1 CA pentamer and comparison with the hexamer

a, Top view of the pentamer, with the NTD colored in orange and the CTD in blue. Helices are represented as cylinders. **b, c,** Top view (b) and side view (c) of the pentamer, with the helices as ribbons. Each subunit is in a different color. **d, e, f,** Equivalent views of the hexamer (PDB code: 3H4E)11. The yellow spheres in (a) and (d) indicate the positions of the pentamer-stabilizing (N21C/A22C) and hexamer-stabilizing (A14C/E45C) disulfide bonds, respectively.

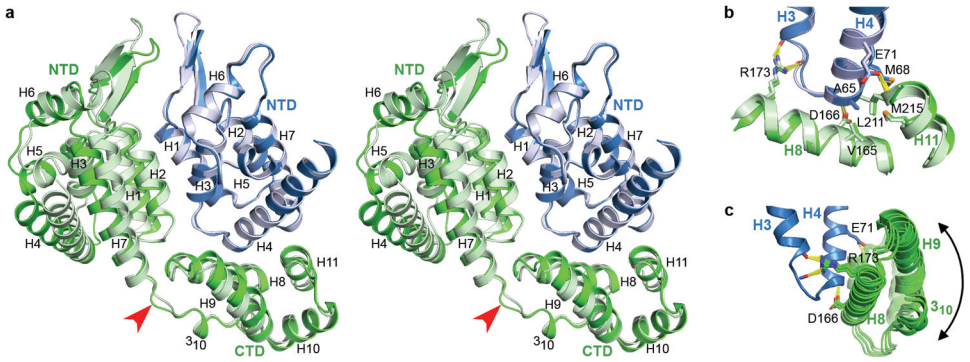

Figure 2. Comparison of the pentamer and hexamer interactions

Both oligomers are created by quasi-equivalent packing of each of the two domains of one CA subunit (colored in green) with the NTD of a second subunit (blue). **a,** Stereoview superposition of the pentamer interface (dark colors) and the hexamer interface (light colors). The structures are superimposed on the blue NTD. **b,** Close-up view of representative NTD-CTD contact regions in the pentamer and hexamer. Key residues are shown explicitly and labeled, with hydrogen bonds colored in yellow. **c,** Comparison of crystallographically independent NTD-CTD interfaces in the pentamer, superimposed on the NTD. Flexion of the two domains is indicated by the black double-headed arrow, and occurs about molecular pivots composed of intermolecular helix-capping hydrogen bonds. The relevant side chains are shown explicitly and labeled, and hydrogen bonds are indicated by yellow lines.

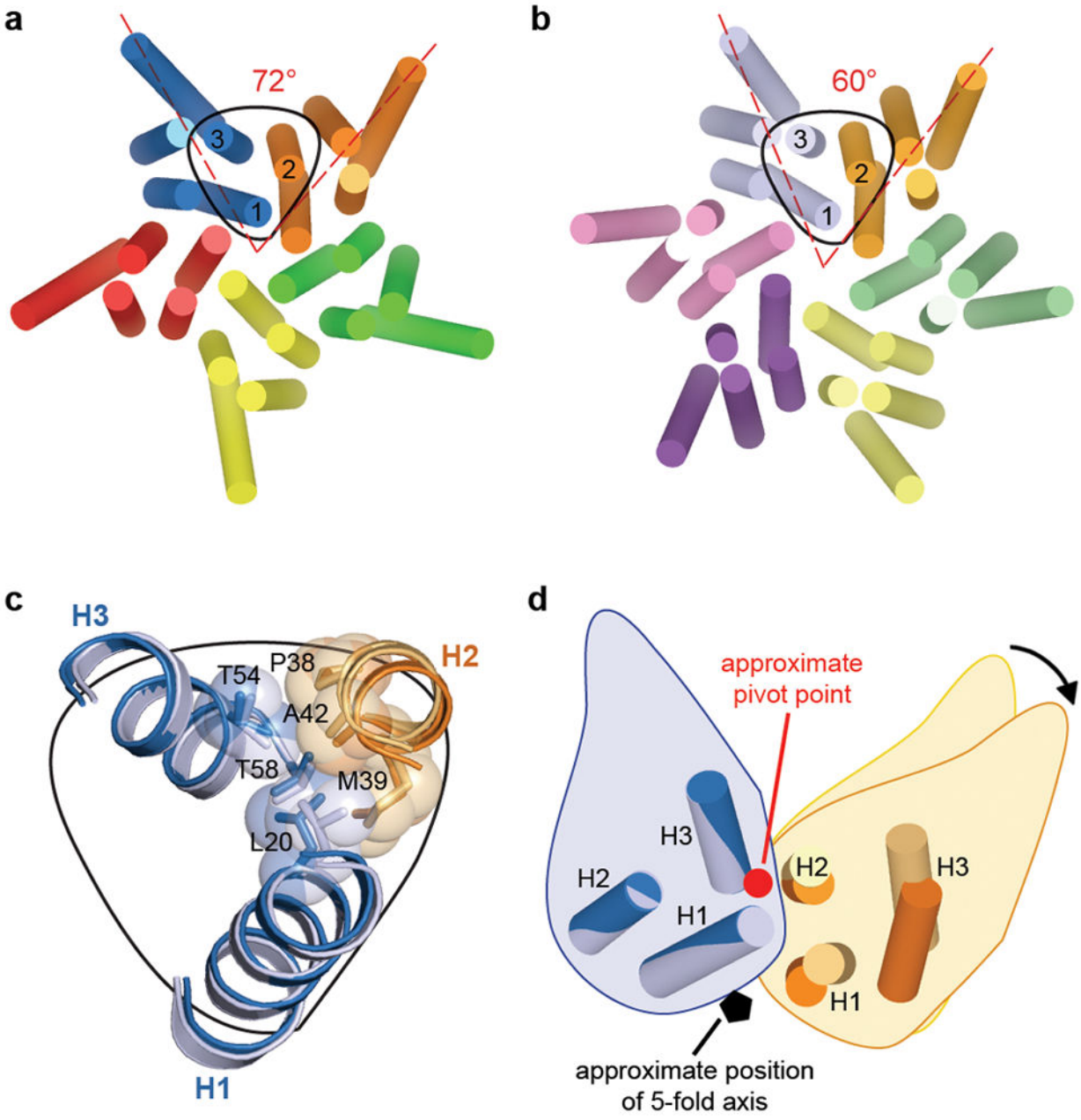

Figure 3. Quasi-equivalence in the pentameric and hexameric NTD rings

a, b, Top views of the pentameric (a) and hexameric (b) NTD rings, with each subunit in a different color. Subunits in the pentamer and hexamer are shown in darker and lighter shades, respectively. The angles subtended by adjacent domains are shown explicitly for the blue and orange subunits. One of the repeating 3-helix units is outlined in black. **c,** Close-up view of the pentameric and hexameric repeat units, superimposed on helices 1 and 3 of the blue subunit. The aliphatic residues that form a small hydrophobic core are shown explicitly and labeled. **d,** Illustration of the "rotation" between adjacent subunits, in going from the hexamer to the pentamer. The approximate position of the rotation axis is indicated by the

red dot. Note that this axis is parallel to neither the pentameric nor hexameric symmetry axes.

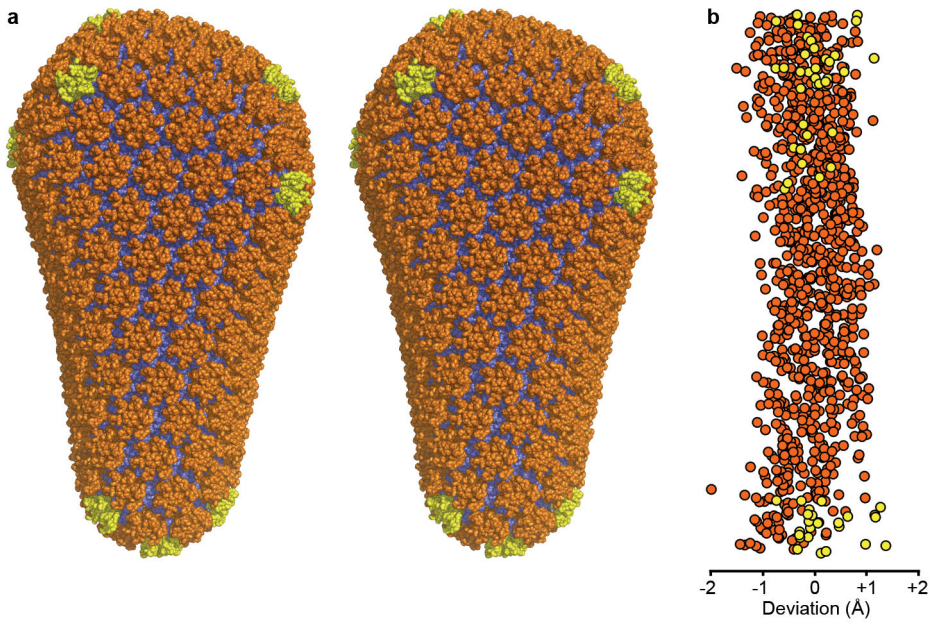

Figure 4. Model of the HIV-1 capsid

a, Stereoview of a backbone-only fullerene cone model composed of 1,056 CA subunits. The hexamers, pentamers, and dimers are colored in orange, yellow, and blue, respectively. Note that the capsid displays a variably curved surface. In the body of the cone, curvature changes continually, and this was modeled by means of subunit flexion at the NTD-CTD interface. Pentamers alter the trajectory of the hexagonal lattice and create regions of sharp curvature (i.e., declinations). Exactly 12 declinations are required to close a hexagonal lattice. Our modeling suggests that formation of the declinations entails a flexible CTD dimer. Note also that the CTD subunits surrounding the local 3-fold axes are in close proximity, consistent with the finding that this site constitutes a fourth set of capsid-stabilizing interactions12. **b,** Graph showing the extent by which the intersubunit distances across the modeled NTD-CTD interfaces deviate from the expected value, as a function of cone length (deviation = $\text{distance}_{\text{modeled}} - \text{distance}_{\text{expected}}$, where $\text{distance}_{\text{expected}} = 9.0$ Å, and refers to the average separation of hydrogen-bonded pairs in the X-ray structures of the hexameric and pentameric NTD-CTD interfaces) (see Methods for details). Note that 99% of the NTD-CTD distances in the model are within 1 A of the expected value. This suggests that the model is of good quality, in light of the sizeable number of constraints imposed on the subunit interactions.